Preprints, 10th IFAC International Symposium on
Advances in Automotive Control
Columbus, Ohio, USA, August 28-30, 2022

State of Charge Estimation for Lithium-ion Batteries using Extreme Learning Machine and Extended Kalman Filter

Zhong Ren* Changqing Du*

* *Hubei Key Laboratory of Advanced Technology for Automotive Components, Wuhan University of Technology, Wuhan 430070, China.*

* *Foshan Xianhu Laboratory of the Advanced Energy Science and Technology Guangdong Laboratory, Foshan 528200, China*

* *Hubei Research Center for New Energy & Intelligent Connected Vehicle, Wuhan University of Technology, Wuhan 430070, China*

(e-mail: renzhong@whut.edu.cn, cq_du@whut.edu.cn)

Abstract: State of charge (SoC) estimation is one of the most important functions for battery management systems (BMSs). Due to the complex electrochemical characteristics of Lithium-ion batteries (LIBs), accurate SoC estimation remain challenges. To take full advantage of the widely used model-based methods and data-driven methods, an extreme learning machine-extended Kalman filter (ELM-EKF)-based method is proposed for SoC estimation in this paper. The ELM is utilized to establish an accurate LIBs model first. Then, the trained ELM model is combined with the EKF algorithm for SoC estimation. The proposed ELM-EKF-based SoC estimation method is validated and compared with the traditional equivalent circuit model-EKF (ECM-EKF)-based method under Federal Urban Driving Schedule (FUDS) driving cycles at three different temperatures. The results prove that the ELM model have better voltage-tracking capability than the ECM model while the ELM-EKF-based SoC estimation algorithm can achieve higher estimation accuracy than the ECM-EKF-based method.

Keywords: Extreme Learning Machine (ELM), Extended Kalman Filter (EKF), Lithium-ion Battery (LIB), State of Charge (SoC)

1. INTRODUCTION

Due to the advantages of high energy density and long lifespan, Lithium-ion Batteries (LIBs) have become the main energy storage medium for electric vehicles (EVs). In order to maintain a stable, safe, and efficient operating condition for battery system, it is critical to develop a battery management system (BMS) whose functions consist of modeling and state estimation, charge and discharge control, thermal management, fault diagnosis and communication with other controllers (Wang et al., 2020). Amongst these functions, state estimation is the most fundamental and crucial one, especially the State of Charge (SoC) estimation. Although SoC serves the same function for EVs as the fuel gauge for petrol-fuel vehicles, it is not a directly measurable value which make it a difficult task for actual applications (Wang et al., 2021).

1.1 Review of SoC Estimation Methods

In the past few decades, numerous researchers have been dedicating to developing advanced SoC estimation methods. So far, the existing SoC estimation methods can be roughly divided into four categories: look-up table-based, Coulomb counting, model-based, and data-driven based methods (Xiong et al., 2017). The look-up table-based methods rely on pre-determined mapping relationship between different parameters and SoC. The main drawback is that accurate online measurements of such parameters have great challenge. Coulomb counting method is widely used in practical applications since it is simply based on the integration of current with respect to time. However, initial SoC error, capacity error, and accumulative error are three main error sources to influence its accuracy. The model-based method draws great popularity for its advantages of high accuracy, self-corrective ability, and relatively simplicity in on-board BMSs. The application procedures of model-based methods usually consist of two parts, namely the battery modeling and SoC estimation algorithms implementation (Shrivastava et al., 2019). As the name suggests, the performance of the model-based methods highly relies on an accurate battery model that can reflect the electrochemical characteristic of LIBs. Typical battery models include electrochemical model (EM), equivalent circuit model (ECM), and fractional order model (FOM). Compared with other battery models, ECM can maintain a trade-off between model complexity and accuracy (Saldaña et al., 2019), thus it is the most used one for model-based SoC estimation methods. As for the SoC estimation algorithms, different filter algorithms, such as Gaussian process-based filter methods including extended Kalman filter (EKF) (Ren et al., 2021), unscented Kalman filter (UKF) (Zhang et al., 2022), sigma-point Kalman filter (SPKF) (Farhaj et al., 2021), and probability-based filter algorithms including particle filter (PF) (Zhengxin et al., 2021), unscented particle filter (UPF) (Wang and Chen, 2020), and cubature particle filter (CPE) (Ling et al., 2021), have been widely used. To

develop an accurate battery model, it is necessary to conduct various battery tests and identify the parameters of the battery model which are usually time-consuming (Ren et al., 2021). The data-driven methods for SoC estimation have become a research hotspot in recent years since they usually consider the LIB as a black box and use various machine learning (ML) methods to map the non-linear relationship between the measured signals and SoC. Some popular ML methods, such as artificial neural network (ANN) (Hannan et al., 2018), deep learning (DL) (Savargaonkar and Chehade, 2020), support vector machine (SVM) (Li et al., 2020), and Gaussian process regression (GPR) (Deng et al., 2020) have been applied for SoC estimation. However, the main disadvantage of the data-driven methods is that these algorithms are sensitive to the quality of the training dataset and may encounter overfitting or underfitting problems easily. In addition, the on-board implementation of data-driven methods for SoC estimation is still a challenge for current stage.

1.2 Motivation and Key Contributions

Although considerable work has been carried out for accurate SoC estimation, there are several limitations in the existing methods. The look-up table based, and Coulomb counting methods are not suitable for long-term practical applications. The model-based methods need considerable time to build an accurate battery model while the data-driven methods may easily encounter overfitting and underfitting problems. To take full advantage of both model-based and data-driven methods, this paper proposes a hybrid strategy for SoC estimation which first uses the extreme learning machine (ELM) to build the battery model. Then, the output of the ELM model is employed as an input of the EKF-based algorithm to estimate SoC. To demonstrate the superiority of the proposed method, the conventional model-based method which combine the Thevenin model with EKF is built for comparison. These two algorithms are validated and compared under dynamic driving cycles at three different temperatures.

1.3 Organization of This Paper

The remainder of this paper is organized as follows: section 2 introduces the experimental setups; section 3 provides the basic theoretical knowledge about the definition of SoC, the ELM model, the Thevenin model and the EKF algorithm; the results and comparison are analyzed in section 4; finally, some conclusions are given in section 5.

2. EXPERIMENT SETUPS

2.1 Experimental Platform

The experimental platform mainly consists of a thermal temperature chamber, a battery test system (Neware BTS-4002) and a host computer for battery test control and data acquisition with 1 s interval. The sampled batteries are 18650 cylindrical graphite $LiNi_{1/3}Co_{1/3}Mn_{1/3}O_2$ batteries with a nominal capacity 2.5Ah and nominal voltage 3.6V.

2.1 Experimental Schedule

To identify the parameters of the Thevenin model, the open circuit voltage (OCV) and hybrid power pulse characterization (HPPC) tests are necessary to conduct. The OCV is a critical parameter for ECM-based SoC estimation algorithms. It represents the terminal voltage of the LIB when it reaches the thermodynamic equilibrium state. The typical steps of OCV test are as follows: (a) The battery is fully charged by means of the constant current–constant voltage (CC-CV) method at the ambient temperature. (b) Rest the battery inside the thermal chamber for 2 hours to reach the thermodynamic equilibrium state and the terminal voltage is considered as the OCV at 100% SoC. (c) The battery is discharged under a constant current with a 1/25-C rate and the terminal voltage is measured every 5% SoC interval. (d) Finally, the terminal voltage reaches the cutoff voltage of 2.5V and then the battery is rested for 2 hours. (e) The battery is charged under a constant current with a 1/25-C rate and the terminal voltage is measured every 5% SoC interval. (f) Finally, when the terminal voltage reaches 4.2V, the average value of charge and discharge terminal voltage is regarded as the OCV since the effects of hysteresis and Ohmic resistance are reduced by the averaging. For the HPPC test, the battery is first fully charged using the CC-CV method at the ambient temperature and then rested inside the thermal chamber at the tested temperatures (10°C, 30°C and 50°C) for 2 hours to reach the thermodynamic equilibrium state. As shown in Fig, 1, the current curve of one HPPC sequence consists of a 30-s constant current discharge, and then a 40-s resting interval followed by a 10-s charge. The battery is discharged with a 1/3-C rate to reach the 5% depth of discharge to the next SoC point and then rested for 1 hour. Repeat the above steps 20 times to cover the whole SoC region.

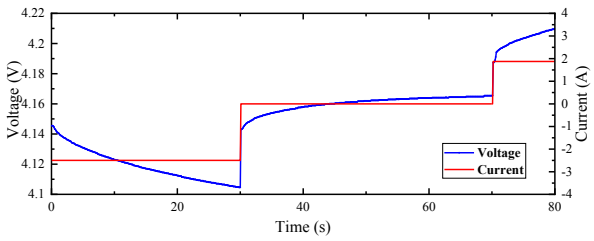

Fig. 1. The current and voltage curves of one HPPC sequence

To validate the battery model and SoC estimation accuracy under dynamic operating conditions, the Federal Urban Driving Schedule (FUDS) test (Anon, 1996), shown in Fig. 2, is conducted at three various temperatures.

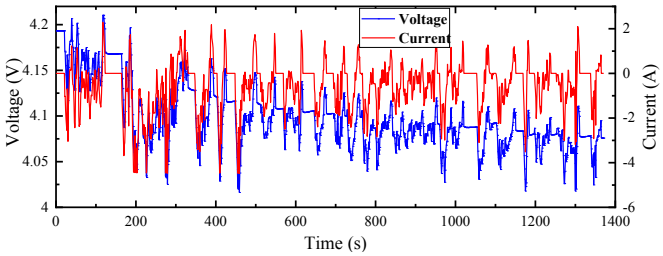

Fig. 2. The voltage and current curves of one FUDS cycle

3. THEORETICAL BACKGROUND

2.1 Definition of State of Charge

SoC represents the remaining amount of available capacity of LIBs which can be expressed as follows

$$SOC(t) = \frac{C_r}{C_m} = SOC(t_0) - \int_{t_0}^{t} \frac{I(t)\eta}{C_m} dt \quad (1)$$

where C_r is the remaining capacity and C_m is the maximum available capacity that a LIB can store, $SOC(t_0)$ represents the initial value, η is the coulombic efficiency and $I(t)$ stands for the current.

2.2 Extreme Learning Machine

ELM is a kind of feed forward neural network (FFNN). Compared with other kinds of FFNN, such as back propagation neural network (BPNN) and radial basic function neural network (RBFNN), ELM has several advantages such as lower computation complexity, faster convergence speed, simpler learning process and good generalization performance (Ding et al., 2015). Thus, ELM is selected in this paper to build the battery model. The structure of ELM is shown in Fig. 3 which contains one input layer, one hidden layer and one output layer. Unlike the BPNN which uses error backpropagation algorithm to train the NN, the learning process of ELM is much simpler which make its superiorities. Considering a dataset defined as $D = \{(x_j, y_j) \mid x_j \in R^n, y_j \in R^m, j = 1, \dots, N\}$, the learning process can be divided into three steps as follows.

(1) Step 1: The input features are selected arbitrarily. Then the input weight vector and hidden layer bias, denoted as $a_i = [a_{i1}, a_{i2}, \dots, a_{in}]^T$ and b_i respectively, are assigned randomly where i stands for the ith hidden layer neuron. The number of hidden neurons is determined flexibly to achieve acceptable accuracy.

(2) Step 2: Use the feed forward propagation algorithm to calculate the output of the ELM. The expressions are as follows

$$\sum_{i=1}^{L} \beta_i f(a_i, b_i, x_j) = y_j, j = 1, \dots, N \quad (2)$$

where $\beta_i = [\beta_{i1}, \beta_{i2}, \dots, \beta_{in}]^T$ represents output weight connecting the ith hidden neuron and output neuron. $f()$ is the activation function of the hidden layer neurons and the widely used sigmoid function is used in this paper.

$$f(a_i, b_i, x_j) = \left(1 + e^{-(a_i \cdot x_j + b_i)}\right)^{-1}, i = 1, \dots, L \quad (3)$$

According to (2), it can be expressed as

$$H\beta = Y \quad (4)$$

where H is the hidden layer matrix.

$$H = \begin{bmatrix} G(a_1, b_1, x_1) & \dots & G(a_L, b_L, x_1) \\ \vdots & \dots & \vdots \\ G(a_1, b_1, x_N) & \dots & G(a_L, b_L, x_N) \end{bmatrix}_{N \times L}$$

$\beta = [\beta_1, \dots, \beta_L]^T$, and $Y = [y_1, \dots, y_N]^T$.

(3) Step 3: The output weights can be analytically determined through the generalized inverse operation of the hidden layer matrix. Therefore, the least square solution is used to calculate the output weight as follows:

$$\beta = H^+ \cdot Y = (H^T H)^{-1} H^T \cdot Y \quad (5)$$

where H^+ the Moore-Penrose generalized invers of H.

It is obvious from the above steps that there is no iteration in the training phase of ELM since it randomly assigns the input weights and hidden layer bias as well as utilizes the Moore-Penrose generalized inverse of pseudoinverse matrix to train the model.

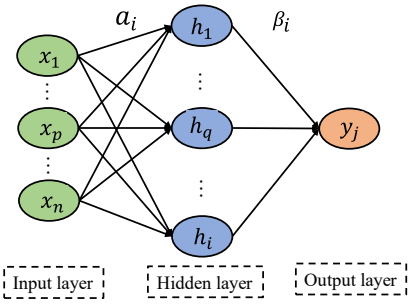

Fig. 3. The structure of ELM

2.2 Extreme Learning Machine Model

Since ELM can map non-linear relationship using input-output samples, thus in this paper, the ELM is used to build a battery model where the $SOC(k)$ and $I(k)$ measured at time step k together with the battery terminal voltage $V(k-1)$ at time step $k-1$ are chosen as inputs while the battery terminal voltage $V(k)$ at time step k is selected as output. Therefore, the expression is shown as follows

$$V(k) = f(V(k-1), I(k), SOC(k)) \quad (6)$$

where f is the mapping function obtained by ELM. According to section 2.1, x_j equals $[V(k-1), I(k), \text{SoC}(k)]^T$ and y_j equals $V(k)$ where n and m equal to 3 and 1 respectively. In addition, the number of hidden neurons is selected as 30 and the training dataset is collected form FUDS test at 30°C while the validation datasets are collected from FUDS test at 10 and 50°C.

2.3 Equivalent Circuit Model

To demonstrate the superiority of the ELM model, the state of art Thevenin model shown in Fig. 4 is built for comparison. The mathematical equations are as follows.

$$U_t = U_{oc} - U_p - R_0 I \quad (7)$$

$$\overline{U_P} = -\frac{U_P}{C_P R_P} + \frac{I}{C_P} \quad (8)$$

where $U_{oc}, R_0, R_P, C_P, U_t, I,$ and U_P represent the OCV, ohmic resistance, polarization resistance, polarization capacitance, terminal voltage, load current, and voltage across the parallel RC network respectively.

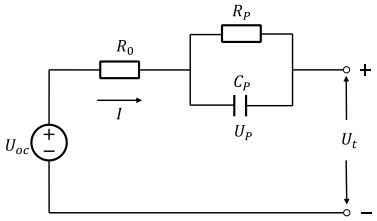

Fig. 4. The Thevenin model

According to the OCV and HPPC tests, the parameters identification results are depicted in Fig. 5. It can be observed that all parameters are sensitive to SoC. Specifically, there is a monotonically increasing relationship between OCV and SoC. But for R_0, in the low or high SoC region, the value of R_0 is much higher indicating poor discharging performance. Same phenomenon can be found in R_P and C_P

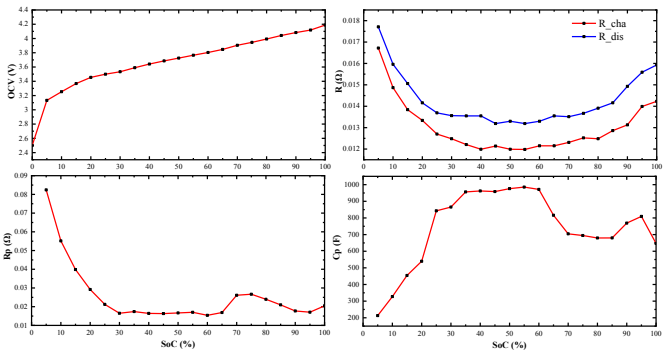

Fig. 5. The parameters identification results of Thevenin model

2.4 Extended Kalman Filter for SoC estimation

The EKF algorithm utilizes the input and output data to recursively optimize the system state. The discretized state-space equations of a nonlinear system can be described as follows:

$$x_{k+1} = f(x_k, u_k) + w_k \tag{9}$$

$$y_k = g(x_k, u_k) + v_k \tag{10}$$

where $x_k \in R^n$ is the state vector, u_k is the input vector, $y_k \in R^m$ is the measured output, w_k and v_k are the process and measurement noises respectively which both are assumed to be mutually uncorrelated white Gaussian random processes with zero mean; $f(x_k, u_k)$ is the nonlinear state transition function and $g(x_k, u_k)$ is the nonlinear measurement function. The recursive process of EKF algorithm is as follows.

(1) Initialization

$$\hat{x}_0^+ = E(x_0),\ P_0^+ = E[(x_0 - \hat{x}_0)(x_0 - \hat{x}_0)^T] \tag{11}$$

(2) Time update

$$\hat{x}_k^- = f(\hat{x}_{k-1}, u_{k-1}) \tag{12}$$

$$P_k^- = A_{k-1} P_{k-1} A_{k-1}^T + Q_k \tag{13}$$

(3) Measurement update

$$K_k = P_k^- C_k^T (C_k P_k^- C_k^T + R_k)^{-1} \tag{14}$$

$$\hat{x}_k^+ = \hat{x}_k^- + K_k[z_k - g(\hat{x}_k^-, u_k)] \tag{15}$$

$$P_k^+ = (I - K_k C_k) P_k^- \tag{16}$$

where K_k is the Kalman gain, P_k is estimation error covariance matrix, z_k is the measurement, A_k and C_k are the Jacobian matrices of the partial derivatives of $f(x_k, u_k)$ and $g(x_k, u_k)$ respectively, Q_k and R_k are process noise and measurement noise covariance matrices respectively. The superscript '−' and '+' represent the prior and posterior estimation respectively.

For different battery models, A_k and C_k have different expressions due to the different $f(x_k, u_k)$ and $g(x_k, u_k)$. According to (2) and (3), the ELM model has the following expression.

$$V(k) = f(x_k) = \sum_{i=1}^{L} \frac{\beta_i}{\left(1+e^{-(a_i[V(k-1), I(k), SOC(k)]^T + b_i)}\right)} \tag{17}$$

Taking the $V(k-1)$ and SoC (k) as state variables in $x_k$and $V(k)$ as the measured output in y_k, the A_k and C_k of ELM model are described as follows.

$$\begin{aligned} A_k &= \frac{\partial f}{\partial x}\Big|_{x=\hat{x}_k} = \begin{bmatrix} \frac{\partial f(x_k))}{\partial x_k} & \\ 0 & 1 \end{bmatrix}\Bigg|_{x=\hat{x}_k} \\ C_k &= \frac{\partial g}{\partial x}\Big|_{x=\hat{x}_k^-} = \begin{bmatrix} \frac{\partial f(x_k)}{\partial x_k} & \\ 0 & 1 \end{bmatrix}\Bigg|_{x=\hat{x}_k^-} \end{aligned} \tag{18}$$

Subsequently,

$$\frac{\partial f(x(k))}{\partial x_k} = \sum_{i=1}^{30} \frac{-\beta_i a_i \left(e^{-(a_i p(k)+b_i)}\right)}{\left(1+e^{-(a_i p(k)+b_i)}\right)^2} \frac{\partial p(k)}{\partial x_k} \tag{19}$$

where

$$\frac{\partial p(k)}{\partial x_k} = \begin{bmatrix} 1 & 0 \\ 0 & 0 \\ 0 & 1 \end{bmatrix}$$

As for the Thevenin model, according to (1), (7), and (8), the discrete forms are as follows.

$$U_{t.k} = U_{oc.k}(SOC) - U_{P.k} - R_{0.k} I_k \tag{20}$$

$$U_{P.k} = U_{P.k-1} \exp\left(\frac{-\Delta t}{\tau_k}\right) + R_{P.k-1}\left(1 - \exp\left(\frac{-\Delta t}{\tau_k}\right)\right) I_{k-1} \tag{21}$$

$$SOC_k = SOC_{k-1} + \frac{\Delta t \cdot \eta \cdot I_k}{C_m \cdot 3600} \tag{22}$$

Therefore, taking the $U_{P.k}$ and SOC_k as state variables and $V(k)$ as the measured output, the A_k and C_k of Thevenin model are described as follows.

$$\begin{aligned} A_k &= \frac{\partial f}{\partial x}\Big|_{x=\hat{x}_k} = \begin{bmatrix} 1 & 0 \\ 0 & \exp\left(\frac{-\Delta t}{\tau_k}\right) \end{bmatrix} \\ C_k &= \frac{\partial g}{\partial x}\Big|_{x_k=x_k^-} = \left[\frac{\partial U_{\mathrm{OCV}}}{\partial \mathrm{SoC}}\Big|_{x_k^-} - 1\right] \end{aligned} \tag{23}$$

4. RESULTS AND DISCUSSTION

4.1 Battery Model Validation

Since an accurate battery model is the premise of EKF-based SoC estimation methods, it is necessary to compared voltage-tracking capability of the ELM and ECM models first. In addition, the mean absolute error (MAE) and root mean square error (RMSE) are employed to quantitatively evaluate the overall performance.

$$MAE = \frac{1}{N}\sum_{k=1}^{N}\left|y_{ref,k} - y_{est,k}\right| \tag{24}$$

$$RMSE = \sqrt{\frac{1}{N}\sum_{k=1}^{N}\left|y_{ref,k} - y_{est,k}\right|^2} \tag{25}$$

where $y_{ref,k}$ is the reference value and $y_{est,k}$ is the estimated value at time step k.

Fig. 6 depicts the voltage-tracking capability of the two models at 30℃. According to Fig. 6(a) which compares the measured and estimated voltages of the two models, it can be observed that both two models can track the measured voltage in the whole range of SoC. However, as shown in Fig. 6(b) which depicts the voltage errors between the measured and estimated voltage, it can be concluded that the ELM model has higher accuracy than the ECM model, especially in the beginning and ending of the test. The voltage errors of the ELM model in the whole range of SoC can remain within 20mV while the errors of the ECM model exceed 50mV approaching the end of the test. According to table 1, the MAEs of the ELM and ECM models are 3.68mV and 12.71mV respectively while the RMSEs are 4.78mV and 17.32mV respectively. In addition, the comparisons of these two models at other temperatures are also given in table 1. Overall, it can be concluded that the ELM model has better voltage-tracking capability than the ECM model.

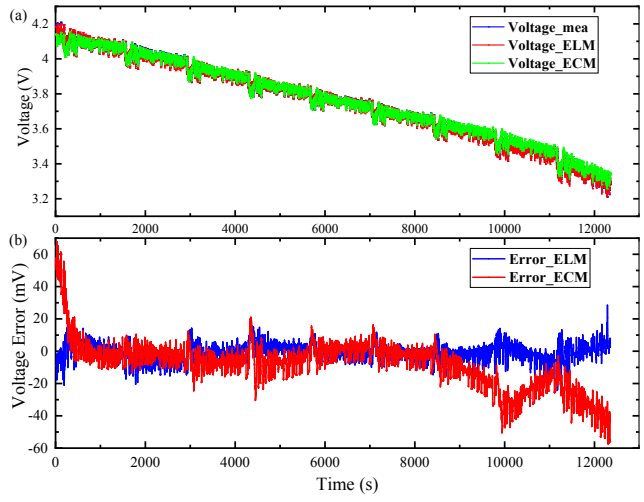

Fig. 6. Comparison of the estimated and measured voltage of the ELM and ECM models at 30℃

Table 1. Model validation results at different temperatures

	Unit: mV	10℃	30℃	50℃
ELM	MAE	8.63	3.68	5.87
	RMSE	12.02	4.78	7.86
ECM	MAE	18.78	12.71	10.44
	RMSE	22.47	17.32	14.13

4.2 SoC Estimation Validation

Fig. 7 depicts the results of two SoC estimation methods, namely the ELM-EKF-based and ECM-EKF-based methods, at 30 ℃. It is unrealistic to know the accurate initial value of SoC in real applications. Thus, the initial value of SoC is set as 75% for both methods although the real value of SoC is 100%. As shown in Fig. 7(a), both two methods can track the reference SoC in the whole range of SoC. In addition, the estimated SoC can converge to the reference SoC quickly in both situations due to the feedback mechanism of EKF algorithm. But the ELM-EKF-based method has the faster convergence rate according to the zoom figure in Fig. 7(a). According to Fig. 7(b) which shows the estimation errors in the whole range of SoC, it can be observed that the estimation errors of ELM-EKF-based method are stable within 2% while the estimation errors of ECM-EKF-based method are much larger, exceeding 5% at around 1000s. According to table 2. the MAEs of the ELM-EKF-based and ECM-EKF-based methods are 0.62% and 1.67% respectively while the RMSEs are 0.95% and 2.39% respectively. Furthermore, the performance of these two methods under other temperatures are compared too. The reason why the ELM-EKF-based method has higher accuracy is that the ELM battery model has better capability in tracking the terminal voltage, thus obtaining small error between the estimated and measured voltage. In addition, the mean Kalman gains of the ELM-based method is smaller than the ECM-based method, indicating that the ELM model outperforms than the ECM model too. Overall, the ELM-EKF-based method outperforms than the ECM-EKF-based method in all temperatures.

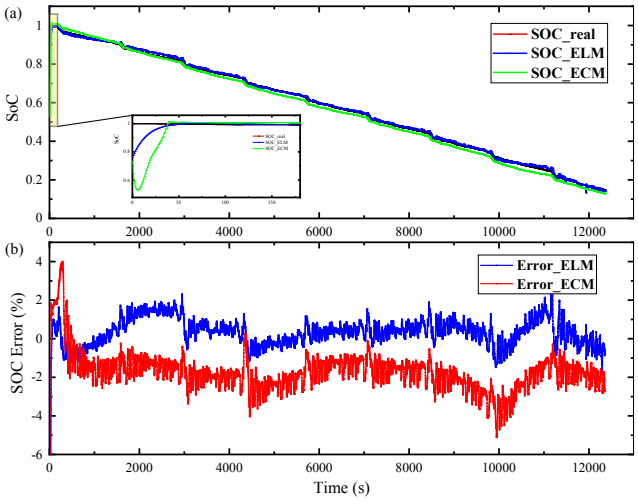

Fig. 7. Comparison of the SoC estimation results of the ELM-EKF-based and ECM-EKF-based methods

Table 2. SoC estimation results at different temperatures

	Unit: %	10°C	30°C	50°C
ELM-EKF	MAE	1.30	0.62	1.4
	RMSE	1.70	0.95	1.68
ECM-EKF	MAE	2.23	1.67	1.96
	RMSE	2.98	2.39	3.58

5. CONCLUSION

In this paper, an ELM-EKF-based method is proposed for SoC estimation where the ELM is utilized to model the battery and then is combined with EKF for SoC estimation. To demonstrate the superiority of the proposed method, traditional Thevenin model based SoC estimation method is built. These two battery models as well as the ELM-EKF-based and ECM-EKF-based SoC estimation methods are validated and compared under FUDS driving cycles at three different temperatures. The results show that the MAE and RMSE of the ELM model are much lower than the ECM model at all temperatuers. Combing with the EKF algorithm, the ELM-EFK-based algorithms can achive hgher SoC estiamtion accuracy than the ECM-EKF-based method at all temperatures too.

The model accuracy can be further improved by considering the aging states since the ELM model can be trained periodically. And the training process of ELM model is relatively easy. The retrained ELM model can be used for SoC estimation fo aging LIBs and guantee an accepatable accuracy.

ACKNOWLEDGEMENTS

This work was supported by Key R&D project of Hubei Province China (grant number 2020BAB132), Foshan Xianhu Laboratory of the Advanced Energyu Science and Technology Guangdong Labpratory (grant number XHD2020-003), and the 111 Project (grant number B17034).

REFERENCES

DENG, Z. et al. (2020) Data-driven state of charge estimation for lithium-ion battery packs based on Gaussian process regression. *Energy*, 205, [Online] Available from: doi.org/10.1016/j.energy.2020.118000.

DING, S. et al. (2015) Extreme learning machine: algorithm, theory and applications. *Artificial Intelligence Review*, 44(1), 103–115.

FARHAJ, H. et al. (2021) A Lagrange multiplier and sigma point Kalman filter based fused methodology for online state of charge estimation of lithium-ion batteries. *Journal of Energy Storage*, 41(August 2020), 102843.

HANNAN, M.A. et al. (2018) Neural network approach for estimating state of charge of lithium-ion battery using backtracking search algorithm. *IEEE Access*, 6, 10069–10079.

LI, R. et al. (2020) State of charge prediction algorithm of lithium-ion battery based on PSO-SVR cross validation. *IEEE Access*, 8, 10234–10242.

LING, L. et al. (2021) State of charge estimation of Lithium-ion batteries based on the probabilistic fusion of two kinds of cubature Kalman filters. *Journal of Energy Storage*, 43(March), 103070.

REN, Z. et al. (2021) A comparative study of the influence of different open circuit voltage tests on model-based state of charge estimation for lithium-ion batteries. *International Journal of Energy Research*, 45(9), 13692–13711.

SALDAÑA, G. et al. (2019) Analysis of the current electric battery models for electric vehicle simulation. *Energies*, 12(14), [Online] Available from: doi.org/10.3390/en12142750.

SAVARGAONKAR, M. and CHEHADE, A. (2020) An adaptive deep neural network with transfer learning for state-of-charge estimations of battery cells. *2020 IEEE Transportation Electrification Conference and Expo, ITEC 2020*, 598–602.

SHRIVASTAVA, P. et al. (2019) Overview of model-based online state-of-charge estimation using Kalman filter family for lithium-ion batteries. *Renewable and Sustainable Energy Reviews*, 113(December 2018), 109233.

USABC Electric Vehicle Battery Test Procedures Manual Revision 2. (1996).

WANG, Y. et al. (2020) A comprehensive review of battery modeling and state estimation approaches for advanced battery management systems. *Renewable and Sustainable Energy Reviews*, 131(March), 110015.

WANG, Y. and CHEN, Z. (2020) A framework for state-of-charge and remaining discharge time prediction using unscented particle fi lter. *Applied Energy*, 260(November 2019), 114324.

WANG, Z. et al. (2021) A review on online state of charge and state of health estimation for lithium-ion batteries in electric vehicles. *Energy Reports*, 7, 5141–5161.

XIONG, R. et al. (2017) Critical Review on the Battery State of Charge Estimation Methods for Electric Vehicles. *IEEE Access*, 6, 1832–1843.

ZHANG, S. et al. (2022) A comparative study of different adaptive extended/unscented Kalman filters for lithium-ion battery state-of-charge estimation. *Energy*, 246, 123423.

ZHENGXIN, J. et al. (2021) An Immune Genetic Extended Kalman Particle Filter approach on state of charge estimation for lithium-ion battery. *Energy*, 230, 120805.